Electronic Supplementary Information

Materials

Rhodium(III) acetylacetonate ($Rh(acac)_3$), ruthenium(Ⅲ) acetylacetonate ($Ru(acac)_3$), sodium hydroxide (NaOH), sodium salicylate ($C_7H_5O_3Na$), sodium hypochlorite (NaClO), sodium nitroferricyanide ($C_5FeN_6Na_2O$) were purchased from Shanghai Macklin Biochemical Co., Ltd. Hydrochloric acid (HCl) was obtained from Sinopharm Chemical Reagent Co., Ltd. Ethanol was obtained from Tianjin Fuyu Fine Chemical Co., Ltd. Nafion (5 wt%) solution was obtained from Alfa Aesar (China) Chemical Co., Ltd. Ultrapure water used throughout all experiments was purified through a Ulupure system. All reagents were used as received without further purification.

Apparatus

CHI 760E electrochemical workstation obtained from Shanghai Chenhua Instrument Co., Ltd. X-ray diffraction (XRD) patterns were acquired by using D8 focus diffractometer (BLumker AXS, Germany). Scanning electron microscope (SEM) images were obtained by using field emission SEM (Zeiss, Germany). Transmission electron microscopy (TEM) image was acquired by a JEOL JEM-2100F TEM (Japan). The absorbance data of spectrophotometer were measured on TU-1909 spectrophotometer (Beijing Puxi Instrument Co. Ltd, China).

Preparation of RhRu nanoalloys

The RhRu nanoalloys (RhRu NAs) was prepared by reducing the precursors $Rh(acac)_3$ and $Ru(acac)_3$ with formaldehyde in aqueous solution without any capping agent. The amount of the precursor was 1.25 mg/mL. In a typical synthesis, 6.0 mg $Rh(acac)_3$ and 4.0 mg $Ru(acac)_3$ were dispersed in 8.0 mL ultrapure water under ultrasonic dispersion. Then 1.0 mL of formaldehyde solution was added dropwise, and the mixture became a clear light yellow solution under continuous magnetic stirring. After further stirring for 20 minutes, the clear solution was transferred to a Teflon-lined stainless steel autoclave with a capacity of 20 mL. The sealed autoclave was heated from room temperature to 180°C in 2 hours and maintained at this temperature for 7 hours, and then naturally cooled to room temperature. The resulting black product was

collected by centrifugation (7000 rpm, 5 min) and washed with ethanol several times to remove impurities.

Electrochemical measurement

The RhRu NAs ink was prepared by dispersing 5 mg of RhRu NAs catalyst dispersed into 1 mL ethanol containing 20 μL of 5 wt% Nafion and kept ultrasonic for 1 h. Then 20 μL of the RhRu NAs ink was loaded on the hydrophobic carbon paper (1cm × 1 cm). The RhRu NAs/CP working electrode was prepared well. The hydrophobic carbon paper (CP) surface in this work can facilitate an effective three-phase contact points (TPCPs) for N_2 (gas), electrolyte (liquid), and RhRu nanoalloys (solid).

Prior to the eNRR test, the Nafion membrane was pretreated by heating at 80 °C for 1 hour in 5% H_2O_2 solution and ultrapure water, respectively. Electrochemical measurements were performed in a standard three-electrode system using RhRu NAs/CP as the working electrode, Ag/AgCl as the reference electrode, and graphite rod as the counter electrode. Electrochemical characterization of the RhRu NAs/CP catalysts was carried out in 0.1 M Na2SO4 electrolytes, and the Na_2SO_4 electrolyte was pretreated by high-temperature annealing to eliminate possible nitrate and nitrite pollution according to reports.[1] For the N_2 reduction experiment, the 0.1 M neutral Na_2SO_4 electrolyte was bubbled with N_2 for 30 minutes to form a N_2 saturated environment. eNRR measurement was performed by measuring time-dependent current density curves at different potentials for 2 hours. All experiments were carried out at room temperature (25 °C).

Determination of NH_3

The produced ammonia was estimated by indophenol blue method by ultraviolet spectroscopy.[2] In detail, 4 mL electrolyte was removed from the cathodic chamber and added into 50 μL oxidizing solution containing NaClO (ρCl =4–4.9) and NaOH (0.75 M), followed by further adding 500 μL coloring solution containing 0.4 M $C_7H_5O_3Na$ and 0.32 M NaOH, and 50 μL catalyst solution (0.1 g $Na_2[Fe(CN)_5NO]\cdot H_2O$ diluted to 10 mL with deionized water) in turn. After standing at 25 °C for 2 hours, the UV-Vis absorption spectrum was measured. The concentration of indophenol blue was determined using the absorbance at a wavelength of 655 nm. In this study, a

concentration-absorbance curve was obtained using a standard ammonium chloride solution firstly. The fitted curve ($y = 0.067 + 0.49x$, $R^2 = 0.999$) indicates a good linear relationship between the absorbance value and the NH_3 concentration. Next, electrolyte was obtained from the electrochemical reaction cathode vessel for UV-Vis spectrometry.

Determination of N_2H_4

The possible by-product N_2H_4 was measured by spectrophotometry with dimethylaminobenzaldehyde.[3] A mixed solution of p-$C_9H_{11}NO$ (5.99 g), HCI (30 mL), and C_2H_5OH (300 mL) was used as a color reagent. In detail, 5 mL of the prepared chromogenic reagent was added to the solution to be tested and stirred at 25 °C for 15 minutes. As with the determination of the main product NH_3, the concentration-absorbance calibration curve was first obtained ($y = 0.04 + 0.7x$, $R^2 = 0.999$), and then the absorbance of the electrochemical reactor cathode electrolyte solution was determined.

Calculations of NH_3 formation rate and FE

Rate of NH_3 formation was calculated using the following equation:

$$R_{NH_3} = \frac{c_{NH_3} \times V}{17 \times t \times m_{cat.}}$$

FE was calculated according to following equation:

$$FE = \frac{3F \times c_{NH_3} \times V}{17 \times Q}$$

Where c_{NH_3} is the measured NH_3 concentration; V is the volume of the cathodic reaction electrolyte; t is the potential applied time; m is the loaded quality of catalyst; F is the Faraday constant (96500 C mol^{-1}); and Q is the quantity of applied electricity.

Computational methods and details

All DFT calculations were carried out using the Vienna Ab-initio Simulation Package (VASP).[4, 5] The exchange and correlation function was described by the generalized gradient approximation (GGA) with Perdew-Burke-Ernzerhof (PBE).[6] The interaction between valence electron and ion core was treated by the projector-

augmented wave method (PAW).[7] The cutoff of kinetic energy was 450 eV and the total energy was converged to less than 10^{-5} eV. All surfaces were optimized using Monkhorst-Pack[8] k-points of 3×3×1, which was tested to be sufficient for convergence to less than 0.001 eV/atom. The vacuum layer of 15 Å thickness was set to avoid the periodic interaction. The atomic positions were optimized until the force on each atom was less 0.02 eV/Å. Van der Waals (vdW) correction by Grimme's DFT-D3 method[9] was further added to describe the non-bonded interaction of the systems. Dipole correction along the slab normal has also been considered.[10]

Herein, we mainly considered the N_2 reduction process on the the RhRu(111) with a Rh:Ru atom ratio of 1:1, Rh(111) and Ru(111) surfaces and first optimized the stable N_2 adsorption configurations as shown in Fig. S19. Based on the the experimental characterization, we constructed the Rh(111) and Ru(111) surfaces with (3×3) four-layer slabs with the top two layers relaxed using experimental lattice parameters of a=b=c=3.83 Å and 3.80 Å for Ru and Rh, respectively. By the Ru substitution in bulk Rh with atom ratio Rh:Ru=1:1, we constructed RhRu(111) surface with (4×4) four-layer slabs that is close to the experimental atomic ratio Rh:Ru=3:2. The Gibbs free energy (G) of a species is calculated by

$$G = E + \mathrm{ZPE} - TS$$

where E is the total energy of adsorbed species from DFT calculations, ZPE and S are the zero-point energy and entropy of a species respectively, and T = 298.15 K. Thermal corrections for gas molecules are from database.[11] Based on the computational hydrogen electrode model,[12] the change in free energy (ΔG) is calculated as

$$\Delta G = \Delta E + \Delta\,\mathrm{ZPE} - T\Delta S$$

The post-processing of VASP calculated data used VASPKIT code.[13] All crystal structures in this article were generated using the VESTA visualization program.[14]

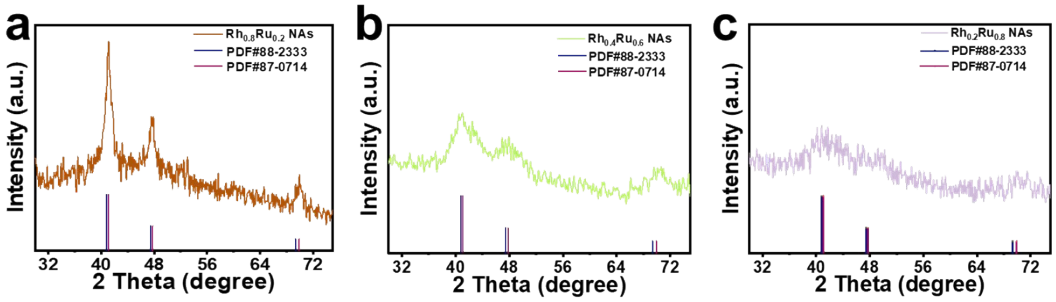

Fig. S1. XRD spectra of (a) $Rh_{0.8}Ru_{0.2}$ NAs, (b) $Rh_{0.4}$ $Ru_{0.6}$ NAs as well as (c) $Rh_{0.2}Ru_{0.8}$ NAs.

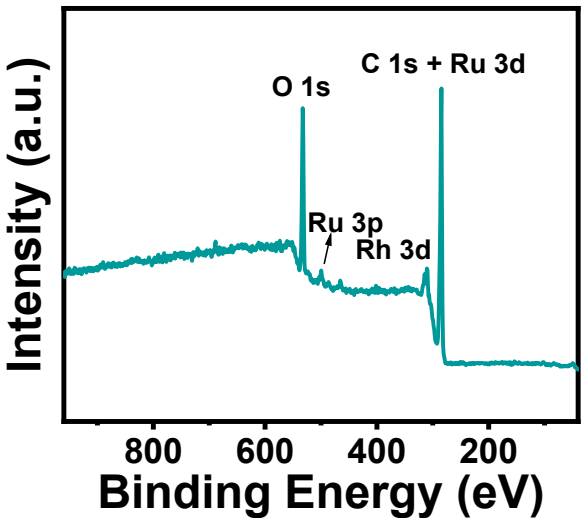

Fig. S2. XPS survey spectrum for $Rh_{0.6}$ $Ru_{0.4}$ NAs.

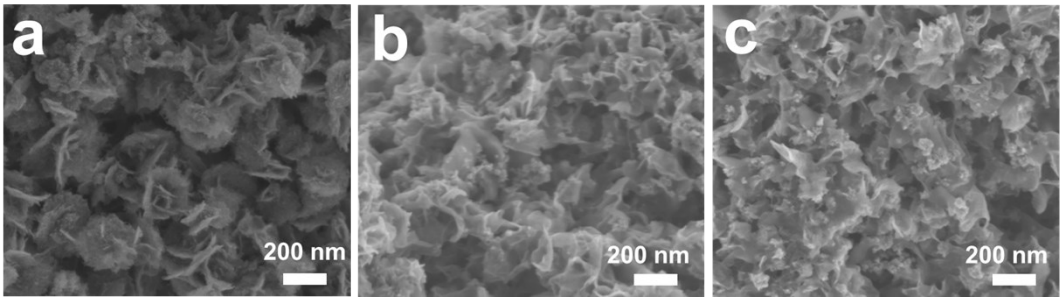

Fig. S3. SEM images of (a) $Rh_{0.8}Ru_{0.2}$ NAs, (b) $Rh_{0.4}$ $Ru_{0.6}$ NAs, and (c) $Rh_{0.2}Ru_{0.8}$ NAs.

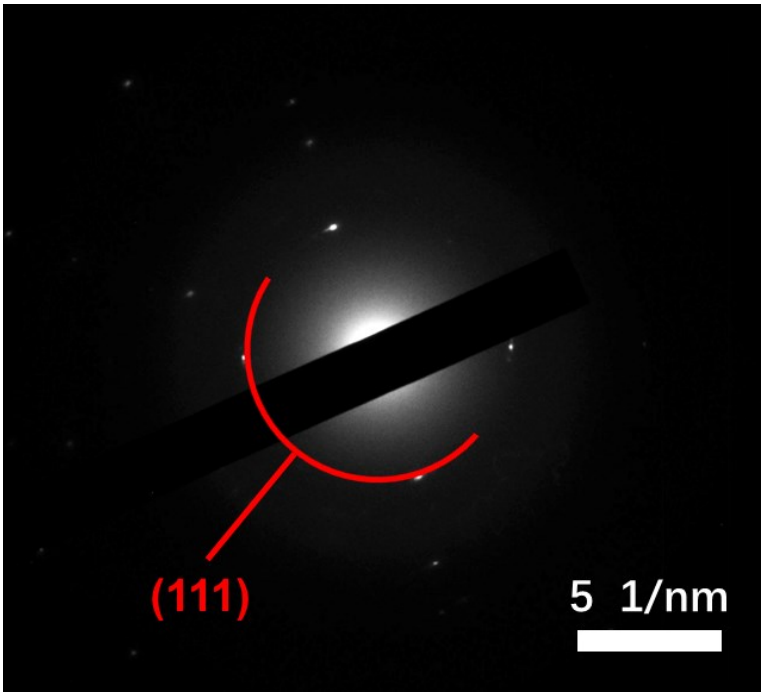

Fig. S4. SAED pattern taken from $Rh_{0.6}Ru_{0.4}$ NAs.

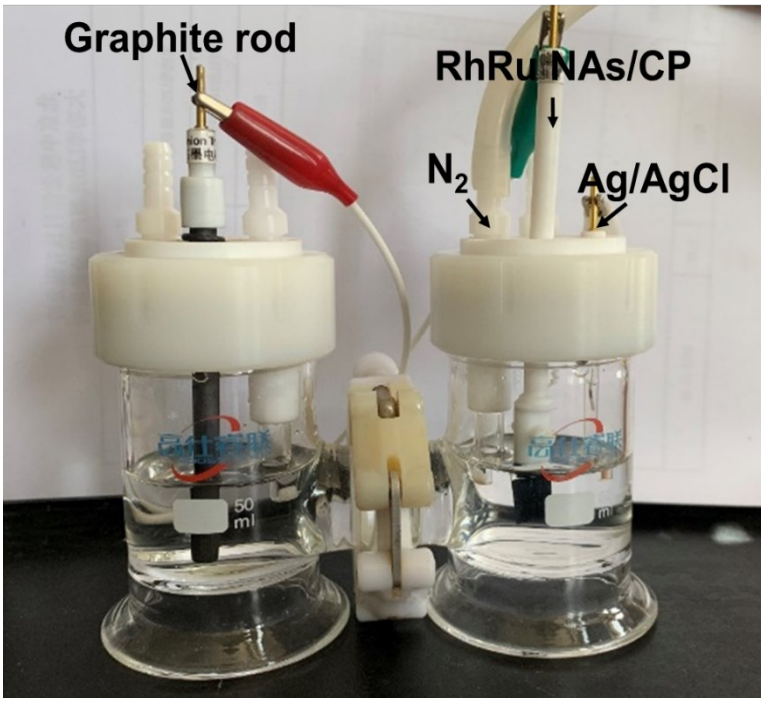

Fig. S5. Optical photograph of the electrocatalytic device used in the eNRR process.

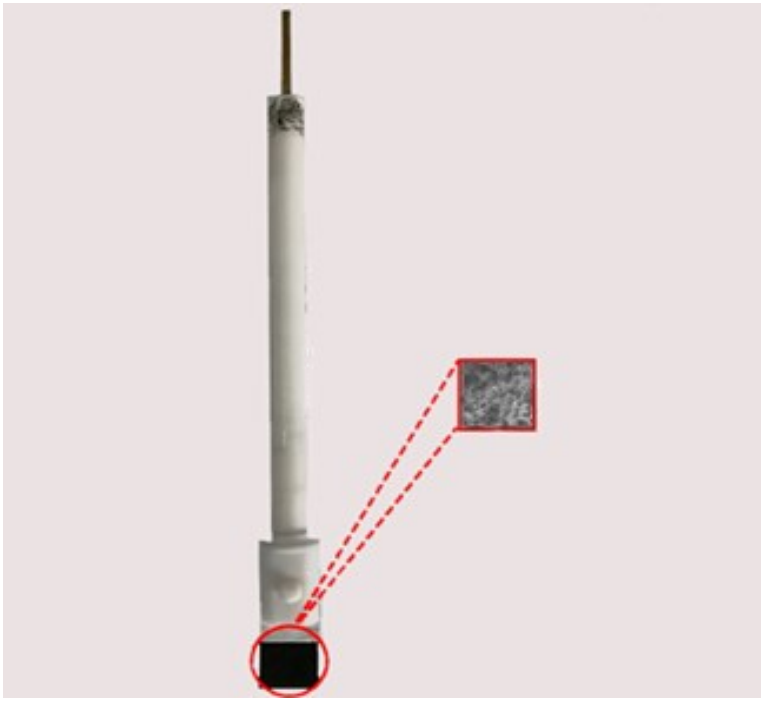

Fig. S6. Optical photograph of the prepared cathode.

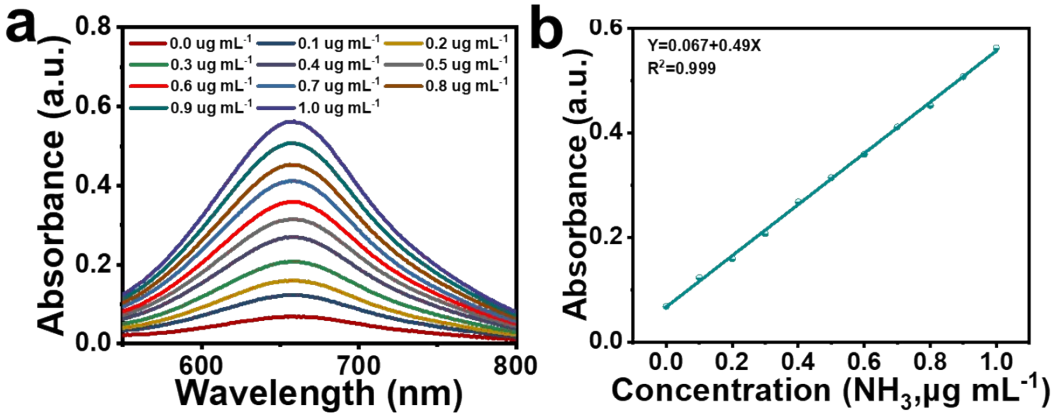

Fig. S7. (a) UV-Vis absorption spectra of various concentrations of NH_3 stained with indophenol indicator. (b) Calibration curve used for estimation of NH_3 concentrations.

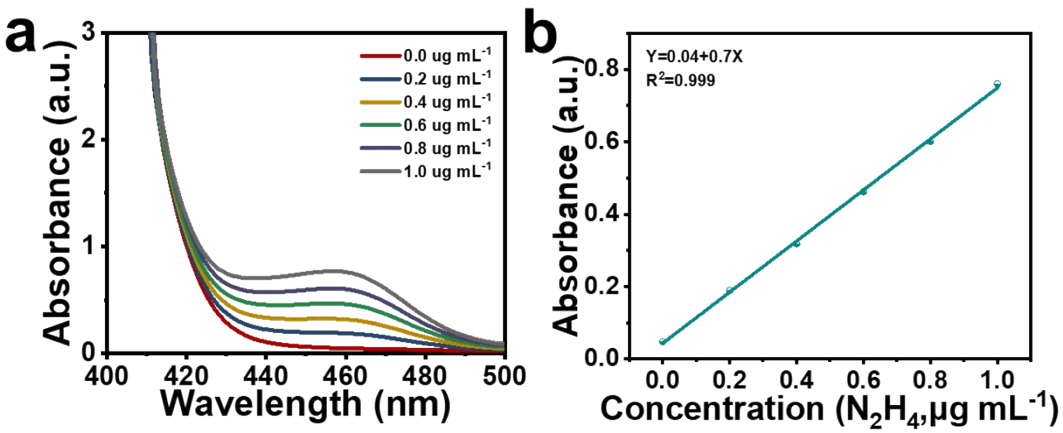

Fig. S8. (a) UV-Vis absorption spectra of various concentrations of N_2H_4 stained with N_2H_4 color agent. (b) Calibration curve used for calculation of N_2H_4 concentrations.

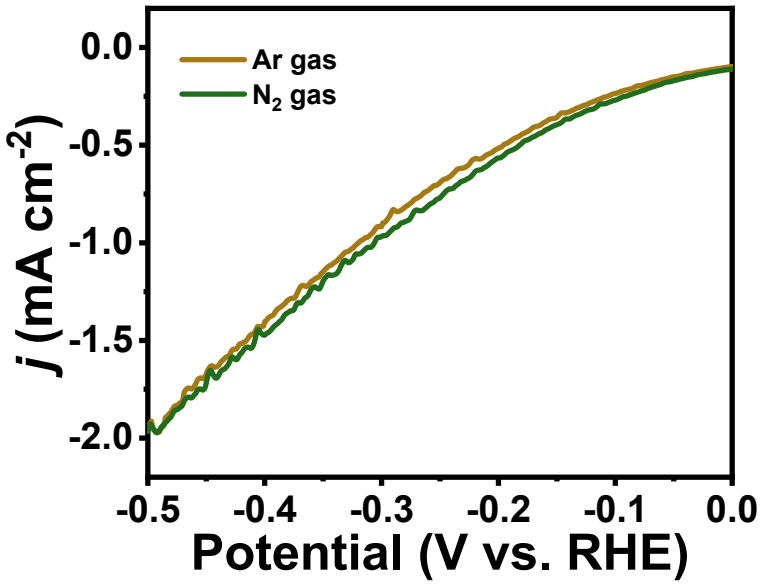

Fig. S9. LSV curves for eNRR test of $Rh_{0.6}Ru_{0.4}$ NAs /CP in Ar-(purple line) and N_2-(green line) saturated electrolytes.

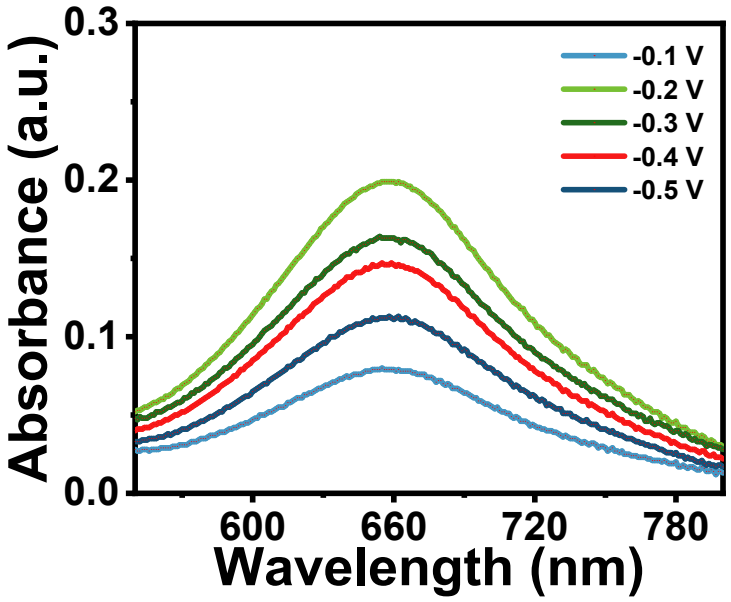

Fig. S10. UV-Vis absorption spectrum of the 0.1 M N_2-saturated Na_2SO_4 electrolyte colored with indophenol indicator after 2 hours electrolysis reactions at different potentials.

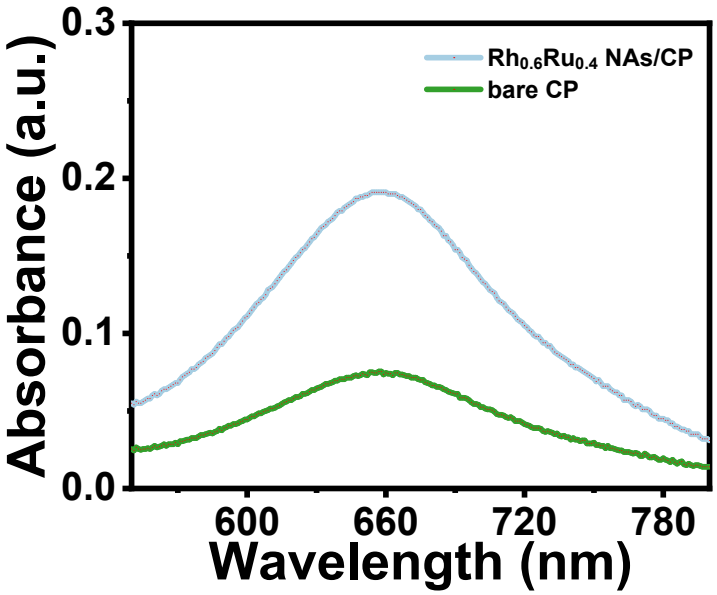

Fig. S11. UV-Vis absorption spectra of electrolytes solution of $Rh_{0.6}Ru_{0.4}$ NAs/CP and bare CP for eNRR test stained with indophenol indicator.

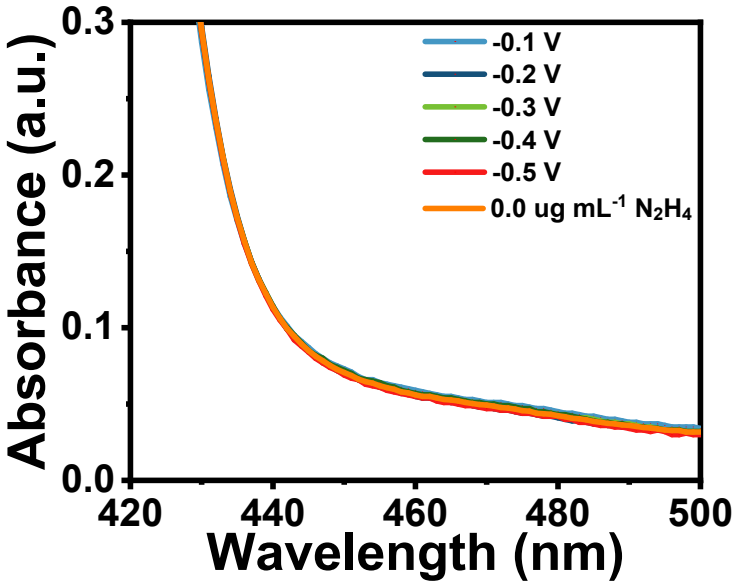

Fig. S12. UV-Vis absorption spectra of electrolyte solution of $Rh_{0.6}Ru_{0.4}$ NAs/CP for eNRR test at each given potentials stained with N_2H_4 color agent.

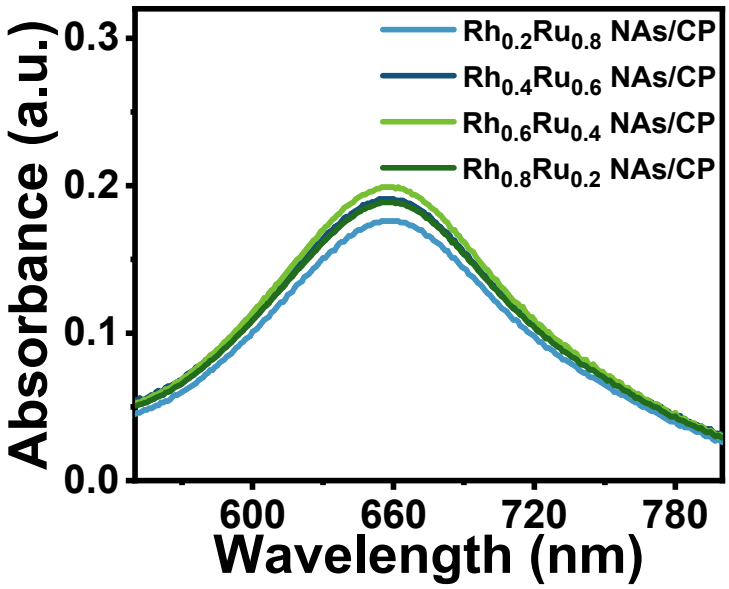

Fig. S13. UV-Vis absorption spectrum of the 0.1 M N_2-saturated Na_2SO_4 electrolyte colored with indophenol indicator after 2 hours eNRR under various Rh/Ru ratio (including $Rh_{0.8}Ru_{0.2}$ NAs/CP, $Rh_{0.6}Ru_{0.4}$ NAs/CP, $Rh_{0.4}Ru_{0.6}$ NAs/CP and $Rh_{0.2}Ru_{0.8}$ NAs/CP).

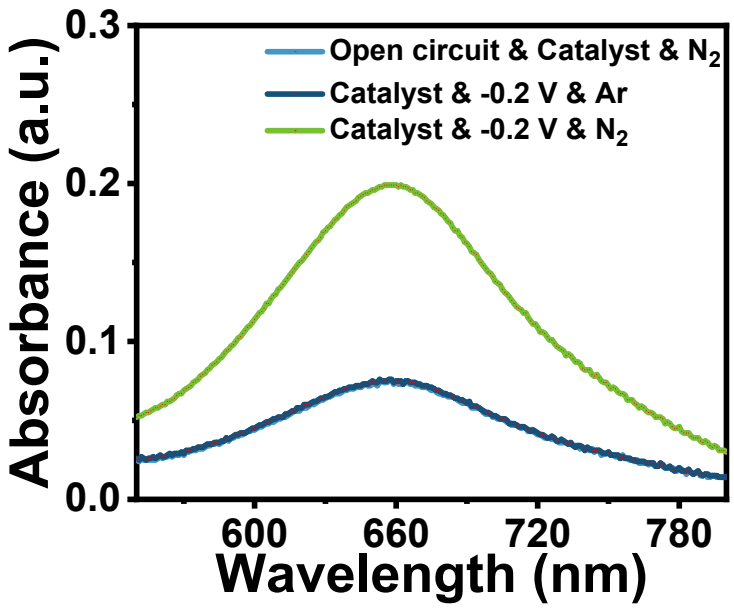

Fig. S14. UV-Vis absorption spectra of electrolytes solution of $Rh_{0.6}Ru_{0.4}$ NAs/CP for eNRR test at different conditions colored with indophenol indicator.

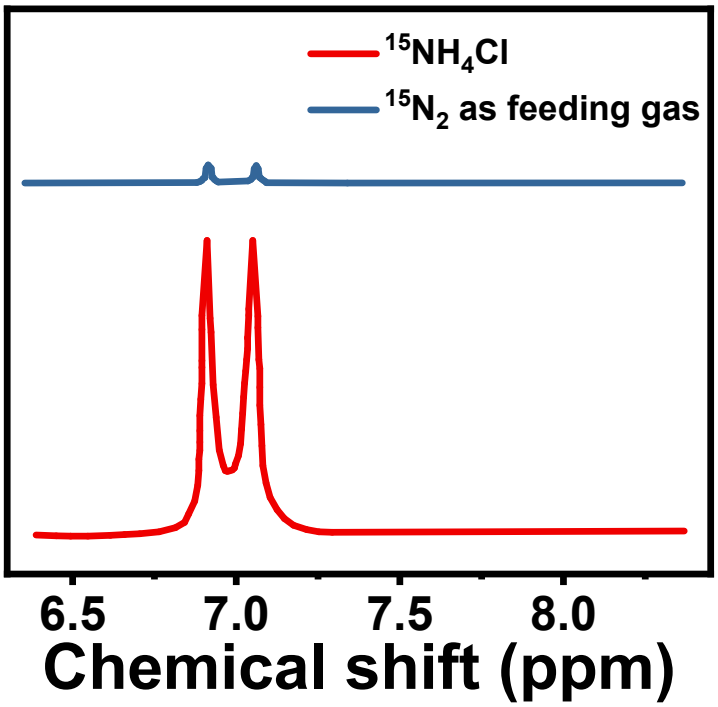

Fig. S15. ^{1}H NMR spectrum of the electrolyte fed by $^{15}N_2$ after the electrolytic reaction at −0.2 V (vs. RHE) for 10 hours. The ^{1}H NMR spectrum for standered $^{15}NH_4Cl$ is also provided for better comparison**.**

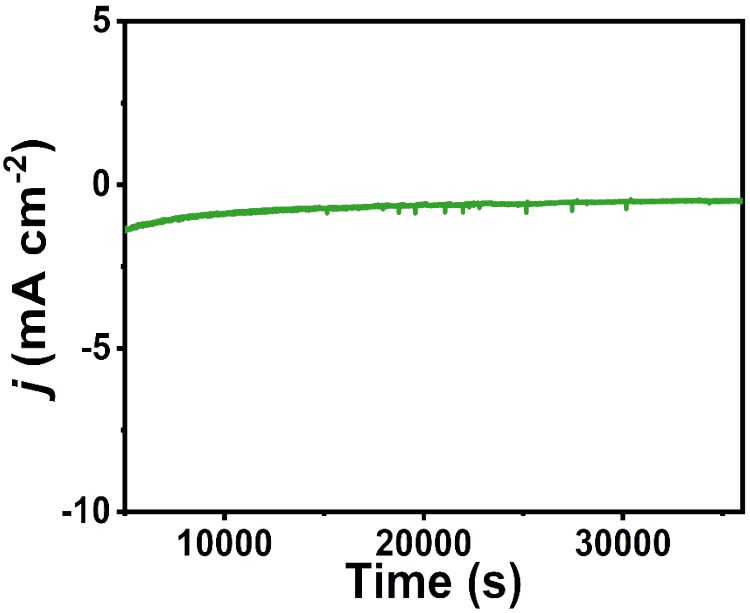

Fig. S16. Time-current density curve using $Rh_{0.6}Ru_{0.4}$ NAs/CP for 12 hours of electrolysis at −0.2 V (vs. RHE).

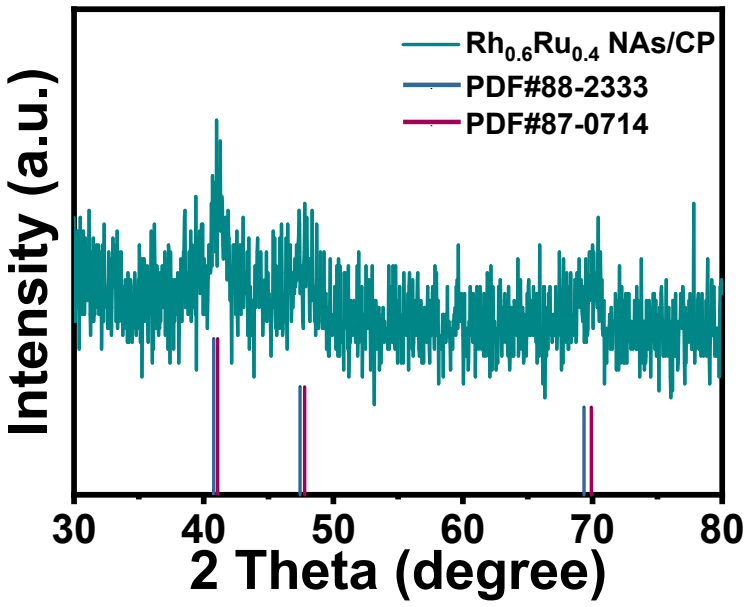

Fig. S17. XRD pattern of $Rh_{0.6}Ru_{0.4}$ NAs/CP after eNRR test at −0.2 V (vs. RHE) for 2 hours.

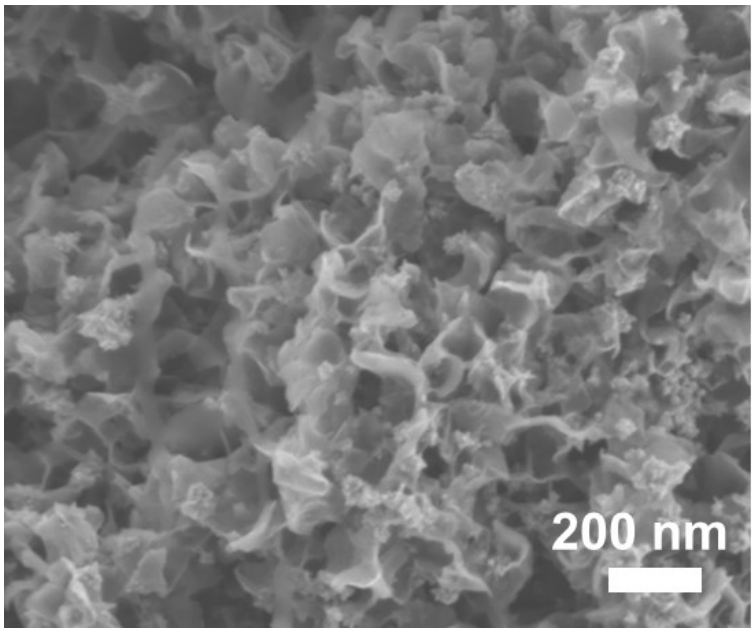

Fig. S18. SEM image of $Rh_{0.6}Ru_{0.4}$ NAs after eNRR test at −0.2 V (vs. RHE) for 2 hours.

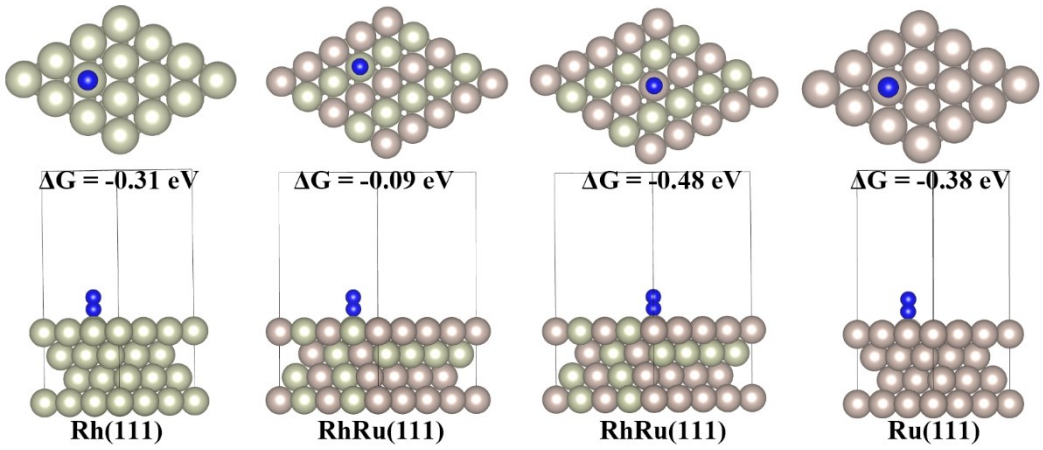

Fig. S19. The optimized configurations and Gibbs free energy changes (ΔG) of N_2 adsorption on top sites of the Rh(111), RhRu(111) with an atom ratio Rh:Ru=1 and Ru(111) surfaces in top and side views.

Table S1. The NH_3 electrosynthesis activity of $Rh_{0.6}Ru_{0.4}$ NAs/CP with other eNRR catalysts under ambient conditions.

Catalyst	Electrolyte	R_{NH_3}	FE	Ref.
$Rh_{0.6}Ru_{0.4}$ NAs/CP	**0.1 M Na_2SO_4**	**57.75 μg h^{-1} $mg^{-1}_{cat.}$**	**3.39 %**	**This work**
TiO_2-rGO	0.1 M Na_2SO_4	15.13 μg h^{-1} $mg^{-1}_{cat.}$	3.3%	[15]
Mn_3O_4 NPs@rGO	0.1 M Na_2SO_4	17.4 μg h^{-1} $mg^{-1}_{cat.}$	3.52%	[16]
Ru NPs	0.1 M HCl	24.88 μg h^{-1} $mg^{-1}_{cat.}$	0.35%	[17]
MoO_3	0.1 M HCl	29.43 μg h^{-1} $mg^{-1}_{cat.}$	1.9%	[18]
PdCu Amorphous Nanocluster	0.1 M KOH	2.8 μg h^{-1} $mg^{-1}_{cat.}$	~0.38 %	[19]
Au nanorods	0.1 M KOH	6.042 μg h^{-1} $mg^{-1}_{cat.}$	4%	[20]
γ-Fe_2O_3	0.1 M KOH	0.212 μg h^{-1} $mg^{-1}_{cat.}$	1.9%	[21]
Pd/C	0.05 M H_2SO_4	2.5 μg h^{-1} $mg^{-1}_{cat.}$	0.1%	[22]
Bi_5O_7Br nanotubes	H_2O	23.46 μg h^{-1} $mg^{-1}_{cat.}$	2.3%	[23]
Fe_3O_4/Ti	0.1 M Na_2SO_4	3.43 μg h^{-1} $cm^{-2}_{cat.}$	2.6%	[24]
MoS_2/CC	0.1 M Na_2SO_4	8.08×10^{-11} mol s^{-1} $cm^{-2}_{cat.}$	1.17%	[25]
Mo nanofilm	0.01 M H_2SO_4	3.09×10^{-11} mol s^{-1} $cm^{-2}_{cat.}$	0.72%	[26]
MoN	0.1 M HCl	3.01×10^{-10} mol s^{-1} $cm^{-2}_{cat.}$	1.15%	[27]
PEBCD/C	0.5 M Li_2SO_4	2.58×10^{-11} mol s^{-1} $cm^{-2}_{cat.}$	2.85%	[28]
Fe_2O_3-CNT	$KHCO_3$	3.58×10^{-12} mol s^{-1} $cm^{-2}_{cat.}$	0.15%	[29]

References:

1. L. Li, C. Tang, D. Yao, Y. Zheng and S.-Z. Qiao, *ACS Energy Lett.*, 2019, **4**, 2111-2116.
2. D. Zhu, L. Zhang, R. E. Ruther and R. J. Hamers, *Nat. Mater.*, 2013, **12**, 836-841.
3. G. W. Watt and J. D. Chrisp, *Anal. Chem.*, 1952, **24**, 2006-2008.
4. G. Kresse and J. Furthmüller, *Phys. Rev. B*, 1996, **54**, 11169-11186.
5. G. Kresse and J. Furthmüller, *Computational Materials Science*, 1996, **6**, 15-50.
6. J. P. Perdew, K. Burke and M. Ernzerhof, *Phys. Rev. Lett.*, 1996, **77**, 3865-3868.
7. P. E. Blöchl, *Phys. Rev. B*, 1994, **50**, 17953-17979.
8. H. J. Monkhorst and J. D. Pack, *Phys. Rev. B*, 1976, **13**, 5188-5192.
9. S. Grimme, J. Antony, S. Ehrlich and H. Krieg, *The Journal of Chemical Physics*, 2010, **132**, 154104.
10. L. Bengtsson, *Phys. Rev. B*, 1999, **59**, 12301-12304.
11. D. R. Lide, *CRC Handbook of Chemistry and Physics, 85th Edition*, Taylor & Francis, 2004.
12. E. Skúlason, T. Bligaard, S. Gudmundsdóttir, F. Studt, J. Rossmeisl, F. Abild-Pedersen, T. Vegge, H. Jónsson and J. K. Nørskov, *Phys. Chem. Chem. Phys.*, 2012, **14**, 1235-1245.
13. V. Wang, N. Xu, J. Liu, G. Tang and W. Geng, VASPKIT: a user-friendly interface facilitating high-throughput computing and analysis using VASP code, https://arxiv.org/abs/1908.08269.
14. K. Momma and F. Izumi, *J. Appl. Crystallogr.*, 2011, **44**, 1272-1276.
15. X. Zhang, Q. Liu, X. Shi, A. M. Asiri, Y. Luo, X. Sun and T. Li, *J. Mater. Chem. A*, 2018, **6**, 17303-17306.
16. H. Huang, F. Gong, Y. Wang, H. Wang, X. Wu, W. Lu, R. Zhao, H. Chen, X. Shi, A. M. Asiri, T. Li, Q. Liu and X. Sun, *Nano Res.*, 2019, **12**, 1093-1098.
17. L. Zhao, J. Zhao, J. Zhao, L. Zhang, D. Wu, H. Wang, J. Li, X. Ren and Q. Wei, *Nanotechnology*, 2020, **31**, 29LT01.
18. J. Han, X. Ji, X. Ren, G. Cui, L. Li, F. Xie, H. Wang, B. Li and X. Sun, *J. Mater.*

Chem. A, 2018, **6**, 12974-12977.

19. M. M. Shi, D. Bao, S. J. Li, B. R. Wulan, J. M. Yan and Q. J. A. E. M. Jiang, *Adv. Energy Mater.*, 2018, **8**, 1800124.
20. D. Bao, Q. Zhang, F. L. Meng, H. X. Zhong, M. M. Shi, Y. Zhang, J. M. Yan, Q. Jiang and X. B. J. A. m. Zhang, *Adv. Mater.*, 2017, **29**, 1604799.
21. J. Kong, A. Lim, C. Yoon, J. H. Jang, H. C. Ham, J. Han, S. Nam, D. Kim, Y.-E. Sung, J. J. A. S. C. Choi and Engineering, *ACS Sustain. Chem. Eng.*, 2017, **5**, 10986-10995.
22. J. Wang, L. Yu, L. Hu, G. Chen, H. Xin and X. Feng, *Nat. Commun.*, 2018, **9**, 1795.
23. S. Wang, X. Hai, X. Ding, K. Chang, Y. Xiang, X. Meng, Z. Yang, H. Chen and J. J. A. M. Ye, *Adv. Mater.*, 2017, **29**, 1701774.
24. Q. Liu, X. Zhang, B. Zhang, Y. Luo, G. Cui, F. Xie and X. J. N. Sun, *Nanoscale*, 2018, **10**, 14386-14389.
25. L. Zhang, X. Ji, X. Ren, Y. Ma, X. Shi, Z. Tian, A. M. Asiri, L. Chen, B. Tang and X. J. A. M. Sun, *Adv. Mater.*, 2018, **30**, 1800191.
26. D. Yang, T. Chen and Z. Wang, *J. Mater. Chem. A*, 2017, **5**, 18967-18971.
27. L. Zhang, X. Ji, X. Ren, Y. Luo, X. Shi, A. M. Asiri, B. Zheng, X. J. A. S. C. Sun and Engineering, *ACS Sustain. Chem. Eng.*, 2018, **6**, 9550-9554.
28. G.-F. Chen, X. Cao, S. Wu, X. Zeng, L.-X. Ding, M. Zhu and H. Wang, *J. Am. Chem. Soc.*, 2017, **139**, 9771-9774.
29. S. Chen, S. Perathoner, C. Ampelli, H. Wei, S. Abate, B. Zhang and G. Centi, *ChemElectroChem*, 2020, **7**, 3028-3037.